Energy Conversion and Management 167 (2018) 63–69

Contents lists available at ScienceDirect

Energy Conversion and Management

journal homepage: www.elsevier.com/locate/enconman

Assessment of the ideality factor on the performance of photovoltaic modules

Caio Meira Amaral da Luz, Fernando Lessa Tofoli*, Paula dos Santos Vicente, Eduardo Moreira Vicente

Federal University of São João del-Rei, Department of Electrical Engineering, Brazil

ARTICLE INFO

Keywords:
Ideality factor
Maximum power point tracking
Photovoltaic modules
Photovoltaic system modeling

ABSTRACT

The ideality factor plays an important role regarding the performance of the photovoltaic (PV) system. Even though several works in literature consider that it remains constant during the system operation, such parameter tends to assume reduced values over time, thus degrading the power that can be extracted from the PV module. It is directly affected by the shunt resistance and, particularly, by the increase of the series resistance due to aging. Besides, it is also influenced by weather conditions, thus causing the corrosion of the PV module cells, manufacturing errors, and "hot spots". Within this context, this paper analyzes the behavior of the ideality factor as influenced by the series resistance. An analytical expression is also presented, as it is possible to evaluate the behavior of the PV module when the ideality factor is reduced as a direct consequence of the aging process. Simulation and experimental results are presented and thoroughly discussed.

1. Introduction

Photovoltaic (PV) modules are internally composed of several series-connected cells, which typically provide low output voltages. With the proper arrangement of modules in series and/or parallel, it is possible to achieve higher voltage and/or current levels as desired. In practice, the *I–V* (current versus voltage) characteristic of a given PV device is nonlinear and depends on both irradiance and temperature [1]. An electric circuit can be used to represent this behavior in the form of the single-diode [2] or double-diode model [3], which are shown in Fig. 1. Although the double-diode one takes into account loss by recombination in the depletion region [4], it consists in a more complete but complex approach [5–7]. On the other hand, the single-diode model has been proven to be precise enough according to literature [8–10], being adopted in this work.

The single-diode model of a PV cell can then be represented by the following well-known expression [11]:

$$I = I_{ph} - I_0\left[e^{\left(\frac{V+R_sI}{AV_t}\right)} - 1\right] - \frac{V + R_sI}{R_{sh}} \quad (1)$$

where I is the cell current; I_{ph} is the photo-generated current; I_0 is the reverse saturation current; V is the cell voltage; R_s and R_{sh} are the series and shunt resistances, respectively; A is the diode quality factor or ideality factor; and V_t is the thermal voltage given by:

$$V_t = \frac{N_s kT}{q} \quad (2)$$

where $k = 1.3806503 \times 10^{-23}$ J/K is the Boltzmann constant; T is the temperature of the p–n junction measured in Kelvin; N_s is the number of series-connected cells per module; and $q = 1.60217646 \times 10^{-19}$C is the electron charge.

Since expression (1) is implicit, several iterative methods have been proposed in order to derive an analytical solution [12]. However, some parameters must be promptly determined for this purpose e.g. R_s and R_{sh}, which are not usually provided by the manufacturer [13]. The series resistance is a lumped parameter representing the summation of several loss mechanisms in a solar cell e.g. losses due to resistance introduced in cell solder bonds, emitter, and base regions, cell metallization, and cell-interconnect busbars [14]. Analogously, the shunt resistance corresponds to any parallel high-conductivity paths across the solar cell p–n junction.

Experimental tests have demonstrated that the reduction of silicon cells efficiency is affected by both the ability of the cell to collect photo-generated carriers and the corresponding increase of the series resistance [15]. The ideality factor of a PV module, as well as other parameters related to the *I–V* curve, also influences the fill factor (FF) and efficiency significantly [16]. In practice, the *I–V* characteristic is

* Corresponding author.
E-mail addresses: caiomeiramaral@hotmail.com (C.M.A. da Luz), fernandolessa@ufsj.edu.br (F.L. Tofoli), paulasantos@ufsj.edu.br (P. dos Santos Vicente), eduardomoreira@ufsj.edu.br (E.M. Vicente).

https://doi.org/10.1016/j.enconman.2018.04.084
Received 7 December 2017; Received in revised form 20 April 2018; Accepted 22 April 2018
Available online 30 April 2018
0196-8904/

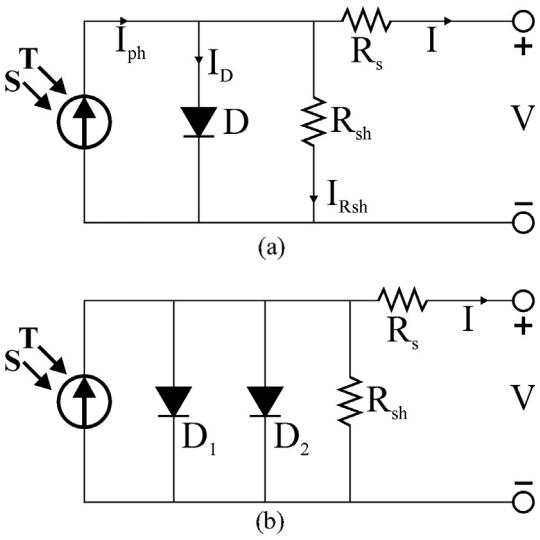

Fig. 1. Representation of the PV module: (a) single-diode model and (b) double-diode model.

not exactly the same as that provided by manufacturers, compromising the extraction of power from the module and the performance of maximum power point techniques (MPPT) [17,18]. Even though it is considered to be constant in several approaches focusing on the modeling of PV modules for computer simulation purposes [11], [19], the ideality factor tends to assume reduced values associated to the aging process of the PV module, thus degrading the useful life of solar cells and operation of the whole PV system.

Literature presents several methods for the estimation of the ideality factor, which are mostly based on the single-diode model, static mode, dc regime, forward bias, and a single *I–V* data set [20]. A thorough review is presented in [20], where it is shown that the accurate determination of intrinsic parameters from experimental data is of major importance for the fabrication process of efficient solar cells [17]. Among 13 evaluated methods, significant advantages and drawbacks for each one of them have been addressed, while it is stated that the ideality factor ranges from 1 to 2 in typical crystalline silicon cells.

The ideality factor represents how accurately the diodes in the PV cell model match the ideal diode equation, what does not occur in practice due to some second-order issues [21]. Considering that it affects the module performance in a real scenario, significant effort has been made in order to adjust *I–V* characteristics obtained by simulation in order to match the real curves as much as possible. Typically, datasheets present relevant information on the module operation, which include the open-circuit voltage (V_{OC}); short-circuit current (I_{SC}); maximum power (P_{MPP}), maximum power voltage (V_{MPP}) and maximum power current (I_{MPP}) under standard test conditions (STC), corresponding to an irradiance level of 1000 W/m^2 and temperature of 25 °C; among other important parameters. According to [2], it is possible to derive a mathematical expression that allows determining the ideality factor from the aforementioned data, although a complex and time-consuming procedure is proposed.

It is worth to mention that some important aspects must be taken into account when experimental measurements regarding the ideality factor are carried out. The shunt resistance R_{sh} influence on *I–V* data is predominant at low voltages and causes appreciable peak, as it is not possible to correct it. On the other hand, the series resistance R_s affects the dark *I–V* curve, being responsible for a large peak in the ideality factor curve in this case. Besides, the measurements are noise prone, as it may be necessary to use curve fitting. The effects of temperature are also of major concern, especially if it comes to vary during the tests.

The influence of R_s, R_{sh}, and the ideality factor on the *I-V* characteristic is quite important for the accurate simulation of PV systems as demonstrated in [22]. Even though an accurate model is presented and validated experimentally for distinct weather conditions, the obtained results do not reflect the module aging process properly since R_s is varied only from 1 mΩ to 1 Ω. It is worth to mention that a significant increase of such parameter is directly related to degradation [15], as it tends to affect the module performance in terms of the maximum power that can be extracted.

The work developed in [23] shows that the series resistance is intrinsically associated to the ideality factor, which represents a measure of how efficiently an applied bias is delivered to the junction of the diode represented in the model of the PV cell. Therefore this aspect must be carefully taken into account, as an approach for the spatial calculation of the ideality factor at the maximum power point is proposed in [24], although it consists in a complex method.

Considering that both R_s and R_{sh} play an important role not only in the modeling of PV modules, but also in the behavior of the ideality factor, this paper is focused on the analysis of the aforementioned parameters and their influence on the *I–V* curve [25]. Firstly, an in-depth discussion on the model that represents PV module is presented, as it is possible to verify the behavior of the photo-generated current, the current through the diode in the model, and the currents through R_s and R_{sh}. Finally, a simple analytical expression can be obtained for the ideality factor, which varies with both resistances associated to the model as demonstrated. Some relevant results are also shown and discussed in detail.

2. Theoretical analysis

2.1. I–V characteristic

The shunt resistance in Fig. 1(a) corresponds to the internal losses associated to the leakage current [26], while the series resistance represents the losses due to voltage drops in metal contacts [15]. Applying the Kirchhoff's current law gives [27]:

$$I = I_{ph} - I_D - I_{Rsh} \tag{3}$$

where I_D is the diode current and I_{Rsh} is the current through R_{sh}.

According to [11], the current generated by the incident light in the module is:

$$I_{ph} = \frac{S}{S_{ref}}[I_{ph(ref)} + k_I(T - T_{ref})] \tag{4}$$

where S and T are the irradiance and temperature of the PV module, respectively; $I_{ph(ref)}$ is the reference photo-generated current at S_{ref} = 1000 W/m^2 and T_{ref} = 25 °C, which correspond to the irradiance and temperature of the PV module under STC; and k_I is the temperature coefficient of the short-circuit current.

It can then be stated that all parameters in (4) are known, except for the irradiance and temperature, which of course depend on weather conditions. The graph in Fig. 2 shows that the photo-generated current increases from 0.61 A to 0.81 A when the temperature varies from 0 °C

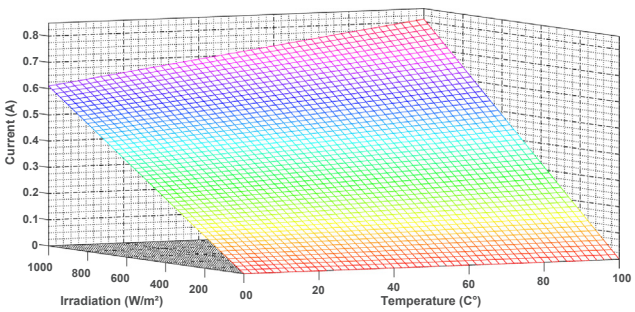

Fig. 2. Behavior of the photogenerated current as a function of the irradiance and temperature for module KM(P)10 by Kyocera®.

to 100 °C, which is due to the dependence of the photo-generated current on parameter k_I. In addition, it can be seen that the photo-generated current varies linearly with the irradiance as in (4).

Besides, the current through the diode in Fig. 1(a) is represented in [27] as:

$$I_D = I_0\left[e^{\left(\frac{V_D}{AV_t}\right)}-1\right] \tag{5}$$

where $V_D = V + R_sI$ is the voltage across the p–n junction.

The reverse saturation current I_0 in (5) can be expressed more accurately considering the influence of temperature on such parameter as in (6):

$$I_0 = I_{0(ref)}\left(\frac{T_{ref}}{T}\right)e^{\left[\frac{qE_g}{Ak}\left(\frac{1}{T_{ref}}-\frac{1}{T}\right)\right]} \tag{6}$$

where $I_{0(ref)}$ is the reverse saturation current under STC; and $E_g = 1.12$ eV is the silicon band-gap energy. Then substituting (6) in (5) gives:

$$I_D = I_{0(ref)}\left(\frac{T_{ref}}{T}\right)e^{\left[\frac{qE_g}{Ak}\left(\frac{1}{T_{ref}}-\frac{1}{T}\right)\right]}\left[e^{\left(\frac{V+R_sI}{AV_t}\right)}-1\right] \tag{7}$$

Besides, the current through the shunt resistance can be determined by applying Ohm's law:

$$I_{Rsh} = \frac{V + R_sI}{R_{sh}} \tag{8}$$

Finally, the current through the module can be obtained substituting (4), (7), and (8) in (3) [27]:

$$I = \frac{S}{S_{ref}}[I_{ph(ref)} + k_I(T-T_{ref})]-I_{0(ref)}\left(\frac{T_{ref}}{T}\right)e^{\left[\frac{qE_g}{Ak}\left(\frac{1}{T_{ref}}-\frac{1}{T}\right)\right]}\left[e^{\left(\frac{V+R_sI}{AV_t}\right)}-1\right] - \frac{V + R_sI}{R_{sh}} \tag{9}$$

In order to plot the *I–V* characteristic from (9) accurately, some intrinsic parameters regarding the PV module must be known, especially R_s and R_{sh}, which can be determined by using either iterative solutions [14] or noniterative ones [28], as the tangent method is adopted in this work for simplicity. The *I-V* characteristic in Fig. 3 is typically provided in datasheets considering STC, from which it is possible to determine R_s and R_{sh} analytically. According to [29], the series and shunt resistances can be obtained from the negative slope of the voltage with respect to the current at $V = V_{OC}$ and $I = I_{SC}$, respectively, as the following expressions are valid:

$$R_s = \tan^{-1}\left(\frac{1}{\beta}\right) \tag{10}$$

$$R_s + R_{sh} = \tan^{-1}\left(\frac{1}{\alpha}\right) \tag{11}$$

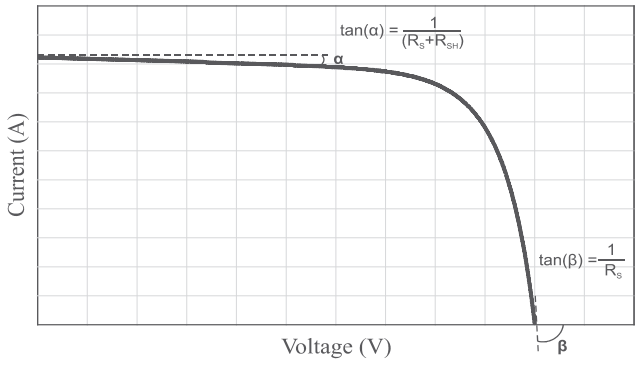

Fig. 3. Estimation of the series and shunt resistances using the tangent method.

where α and β are the angles associated to the tangent lines in the points corresponding to the short-circuit current and open-circuit voltage in the *I–V* characteristic as represented in Fig. 3.

2.2. Ideality factor

In order to determine an analytical expression that provides the ideality factor, the following data provided by the manufacturer are necessary: open-circuit voltage, short-circuit current, as well as the maximum power voltage and current [30]. If the PV module is short-circuited under STC, the following assumptions are valid:

$$T = T_{ref}, S = S_{ref}, I = I_{SC(ref)}, V = 0 \tag{12}$$

where $I_{SC(ref)}$ is the short-circuit current at STC.

If the conditions in (12) are applied to (9), the following expression is obtained:

$$I_{SC(ref)} = I_{ph(ref)}-I_{0(ref)}\left(e^{\frac{R_sI_{SC(ref)}}{AV_t}}-1\right)-\frac{R_sI_{SC(ref)}}{R_{sh}} \tag{13}$$

The work developed in [31] has shown that the reverse saturation current is rated at the order nanoampères. Besides, it is worth to mention that R_{sh} is typically much higher than R_s, thus leading to:

$$I_{SC(ref)} \cong I_{ph(ref)} \tag{14}$$

Analogously, in open-circuit condition under STC, the following assumptions can be made:

$$T = T_{ref}, \quad S = S_{ref}, \quad I = 0, \quad V = V_{OC(ref)} \tag{15}$$

where $V_{OC(ref)}$ is the open-circuit voltage at STC.

Substituting (14) and (15) in (9), it is possible to determine the reverse saturation current under STC as [27]:

$$I_{0(ref)} = \frac{I_{SC(ref)}-\frac{V_{OC(ref)}}{R_{sh}}}{e^{\frac{V_{OC(ref)}}{AV_t}}-1} \tag{16}$$

At the maximum power point under STC, the following parameters can be obtained:

$$T = T_{ref}, S = S_{ref}, I = I_{MPP(ref)}, V = V_{MPP(ref)} \tag{17}$$

where $I_{MPP(ref)}$ and $V_{MPP(ref)}$ are the reference maximum power current and voltage, respectively.

Substituting (14) and (17) in (9) gives [27]:

$$I_{MPP(ref)} = I_{SC(ref)}-I_{0(ref)}\left[e^{\frac{(V_{MPP(ref)}-R_sI_{MPP(ref)})}{AV_t}}-1\right] - \frac{V_{MPP(ref)}-R_sI_{MPP(ref)}}{R_{sh}} \tag{18}$$

Finally, it is possible to obtain the expression that provides the ideality factor substituting (14) and (16) in (18), also taking into account that the exponential terms are much greater than unity as in [27].

$$A = \frac{V_{MPP(ref)}-V_{OC(ref)} + R_sI_{MPP(ref)}}{V_{t(ref)}\ln(B)} \tag{19}$$

where:

$$B = \frac{I_{SC(ref)}-I_{MPP(ref)}-\left(\frac{V_{MPP(ref)}+R_sI_{MPP(ref)}}{R_{sh}}\right)}{I_{SC(ref)}-\frac{V_{OC(ref)}}{R_{sh}}} \tag{20}$$

3. Numerical results

Expression (19) clearly evidences that the ideality factor is influenced by the series and shunt resistances. However, literature shows that such parameters vary with the aging process and, consequently, the ideality factor cannot be considered constant over time [25]. In order to

Table 1
Typical electrical characteristics of PV Module KM(P)10 [32].

Parameter	Value
Maximum power	$P_{max} = 10$ W
Power tolerance	$\Delta P_{max} = 5\%$
Maximum power voltage	$V_{MPP} = 17.56$ V
Maximum power current	$I_{MPP} = 0.6$ A
Open-circuit voltage	$V_{OC} = 21.52$ V
Short-circuit current	$I_{SC} = 0.66$ A
Maximum system voltage	$V_{DC} = 750$ V
Cell efficiency	$\eta = 15.9\%$
Module efficiency	$\eta_{PV} = 10.8\%$
Number of cells per module	$N_s = 36$
Temperature coefficient of I_{sc}	$k_I = +0.05\%/°C/0.00033$ A/°C
Temperature coefficient of V_{oc}	$k_V = -0.34$ mV/°C/-0.0731 V/°C
Temperature coefficient of power	$k_P = -0.5\%/°C$
Nominal operating cell temperature	47 ± 2 °C
Series resistance	$R_s = 0.82\,\Omega$
Shunt resistance	$R_{sh} = 964\,\Omega$

assess this issue properly, module KM(P)10 by KOMAES® is adopted in this work [32], whose electrical parameters given in Table 1 allow obtaining the *I–V* characteristic, and consequently R_s and R_{sh} using the tangent method.

An algorithm has then been developed in software Matlab® as shown in Table 2 to analyze the behavior of the ideality factor. The graph presented in Fig. 4 considers that R_{sh} varies from 1 kΩ to 30 kΩ and R_s varies from 0 Ω to 30 Ω. Besides, it can be stated that $A = 1.7855$ as R_s and R_{sh} tend to zero and infinite, respectively, which corresponds to ideal conditions.

Since the influence of R_{sh} on the ideality factor is not significant in Fig. 4, it is considered constant in the forthcoming analysis. However, Fig. 4 also shows that high values of R_s cause A to become negative. This fact must be carefully taken into account especially considering that R_s tends to increase with aging of the module [33], being this one of the major factors that leads to the degradation of useful life and performance in PV systems [34].

Firstly, let us consider the rated conditions given in Table 1 to plot the *I–V* characteristic of the PV module obtained at 950 W/m^2 and 40 °C as shown in Fig. 5. It is also worth to mention that such weather

Table 2
Source code developed in Matlab® to evaluate the performance of the ideality factor.

```
clc;
clear all;
[Rp, Rs] = meshgrid(1000:0:30000, 0:30);
M = ones(size(Rs));
Icc = 0.66 * M;
Imp = 0.6 * M;
Vca = 21.52 * M;
Vmp = 17.56 * M;
q = 1.602176565e−19 * M;
Eg = 1.2 * M;
k = 1.380648813e−23 * M;
Tref = 298.15 * M;
Ns = 36 * M;
Vrt = (k. * Tref)./q;
% ideality factor;
sup = Icc − Imp − ((Vmp + Rs. * Imp)./Rp);
inf = Icc − Vca./Rp;
n = (Vmp − Vca + Rs. * Imp)./(Vrt. * log(sup./inf));
nl = n./Ns;
mesh(Rs, Rp, nl);
colormap hsv
grid on
xlabel ('Rs')
ylabel ('Rsh')
zlabel ('Ideality Factor')
grid on
```

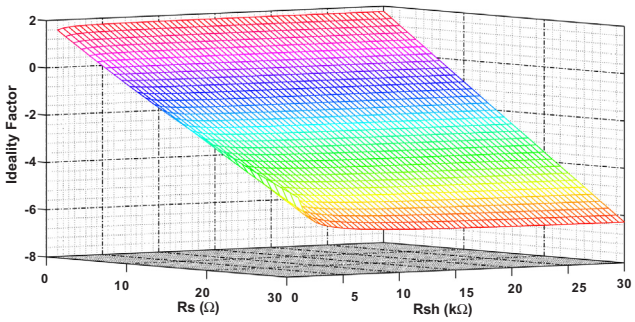

Fig. 4. Influence of R_s and R_{sh} on the ideality factor.

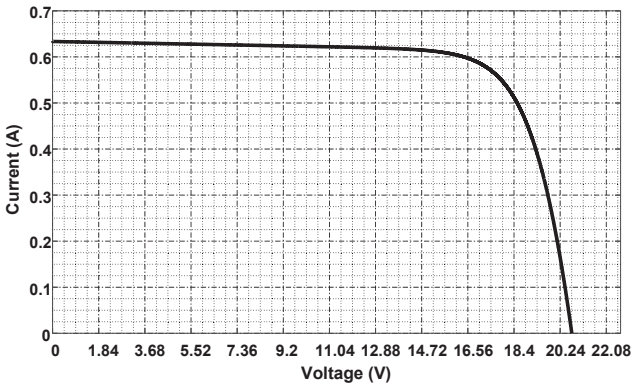

Fig. 5. *I–V* curve for $R_s = 0.82\ \Omega$ and $R_{sh} = 964\,\Omega$ ($S = 950$ W/m^2 and $T = 40$ °C) obtained by simulation.

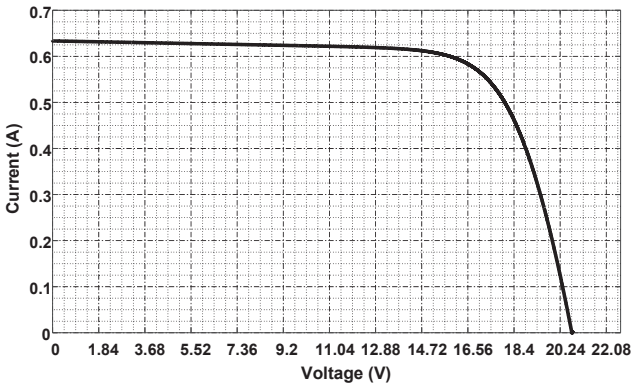

Fig. 6. *I–V* curve for $R_s = 1.82\ \Omega$ and $R_{sh} = 964\,\Omega$ ($S = 950$ W/m^2 and $T = 40$ °C) obtained by simulation.

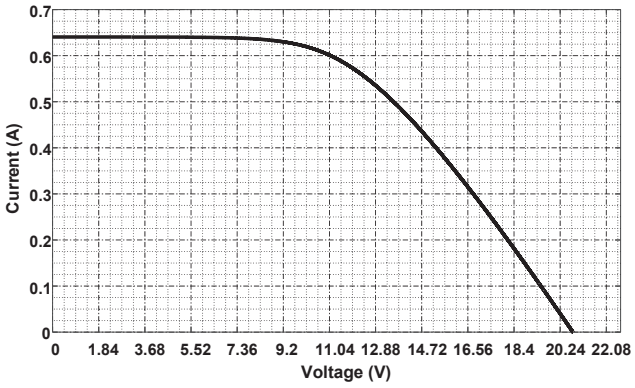

Fig. 7. *I–V* curve for $R_s = 5.82\ \Omega$ and $R_{sh} = 964\,\Omega$ ($S = 950$ W/m^2 and $T = 40$ °C) obtained by simulation.

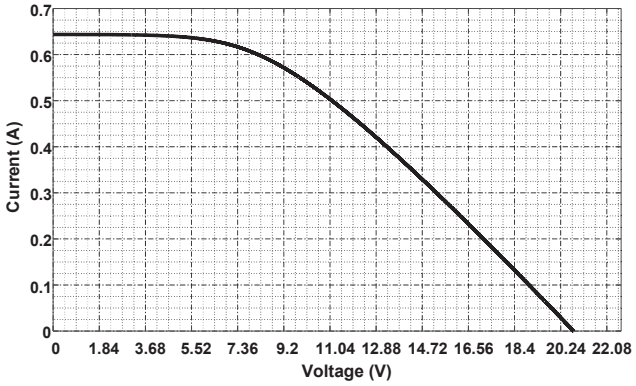

Fig. 8. *I–V* curve for $R_s = 15.82\ \Omega$ and $R_{sh} = 964\,\Omega$ ($S = 950\,W/m^2$ and $T = 40\,^{\circ}C$) obtained by simulation.

conditions have been chosen in the analysis so that a fair comparison can be established between simulation and experimental results.

It can be seen that the increase of the series resistance in Fig. 6 and Fig. 7 implies not only the reduction of the ideality factor to 1.1245 and 0.1778, respectively, but the maximum power to decrease from 9.6704 W and 6.9025 W. With the further increase of R_s over the years, the ideality factor assumes negative values as in Figs. 8 and 9, which may lead to corrosion, degradation, and "hot spots" in practice as stated in [35]. Thus the performance of the whole PV system is compromised considering that the maximum power that can be extracted is significantly reduced.

4. Experimental results

In order to verify the influence of the series resistance in a real system, tests were carried out with distinct values of R_s associated to PV module model KM(P)10 using the experimental setup shown in Fig. 10. Instead of using a solar simulator, outdoor tests were performed, where the weather conditions at that moment corresponded to an irradiance of about $950\,W/m^2$ as measured by Hukseflux pyranometer model SR05. It is worth to mention that both the PV module and the pyranometer remain in the horizontal position during the test session. Besides, the PV module temperature measured with digital infrared thermometer model Fluke 561 at that moment was 40 °C, which was constantly monitored and remained nearly constant. An external fixed resistor is used to emulate the aging process associated to the increase of R_s. On the other hand, a variable resistor rated at 1 kΩ corresponds to the load connected to the PV module, which is quickly varied so that the current and voltage points can be recorded in a flash drive to plot the curves while using voltage and current probes connected to the channels of oscilloscope model DSOX2002A by Keysight.

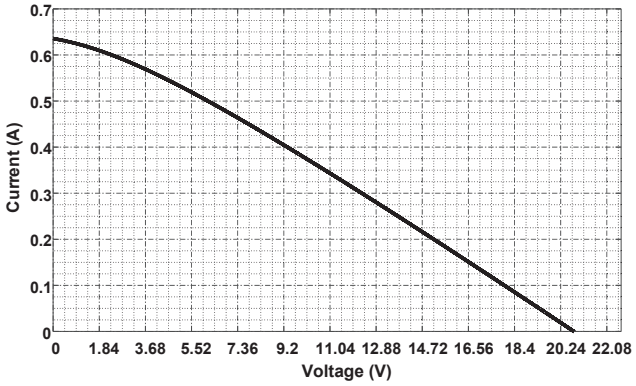

Fig. 9. *I–V* curve for $R_s = 25.82\ \Omega$ and $R_{sh} = 964\,\Omega$ ($S = 950\,W/m^2$ and $T = 40\,^{\circ}C$) obtained by simulation.

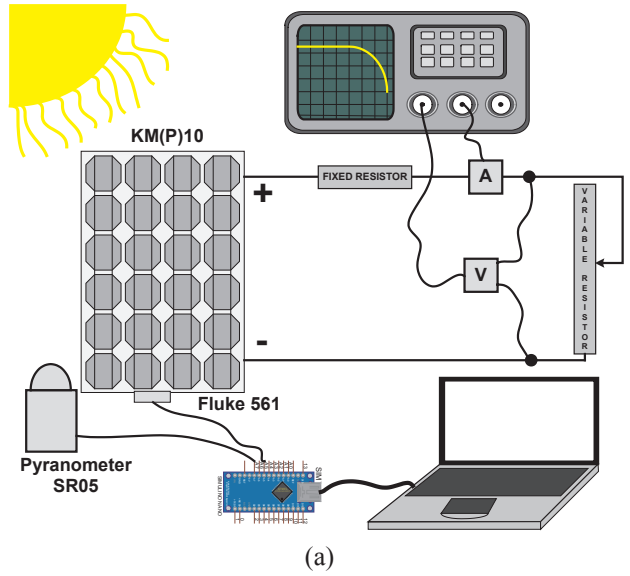

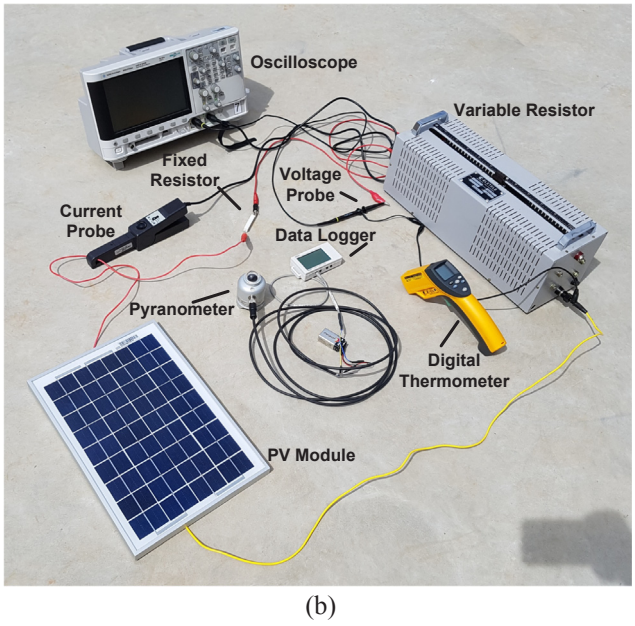

Fig. 10. Experimental setup: (a) general schematic and (b) outdoor tests.

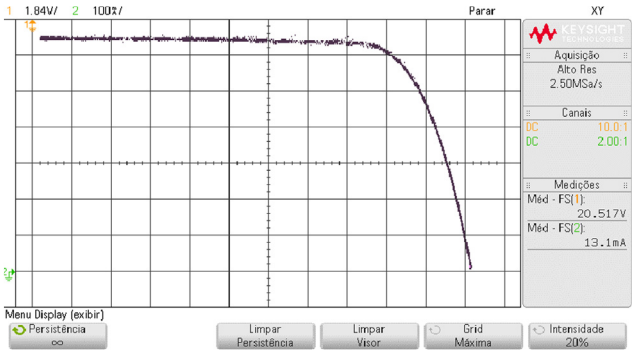

Fig. 11. *I–V* curve for $R_s = 0.82\ \Omega$ ($S = 950\,W/m^2$ and $T = 40\,^{\circ}C$) obtained experimentally.

The *I–V* curve in Fig. 11 has been initially measured, which corresponds to the same conditions valid for Fig. 5. Aging process is emulated using an external resistor rated at 1 Ω to represent the increase of $R_s = 0.82\,\Omega$ to $R_s = 0.82\,\Omega + 1\,\Omega = 1.82\,\Omega$ in Fig. 12, where the

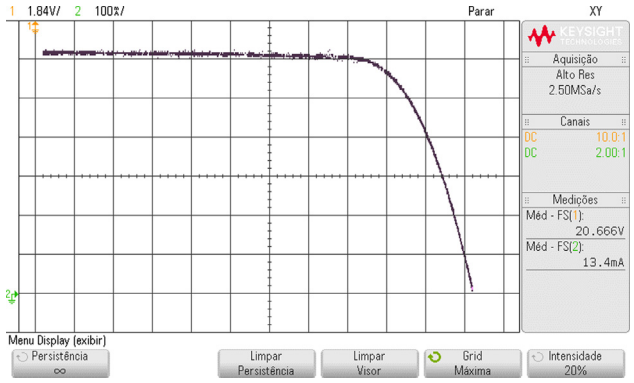

Fig. 12. *I–V* curve for $R_s = 1.82\ \Omega$ and $R_{sh} = 964\,\Omega$ ($S = 950\,W/m^2$ and $T = 40\,°C$) obtained experimentally.

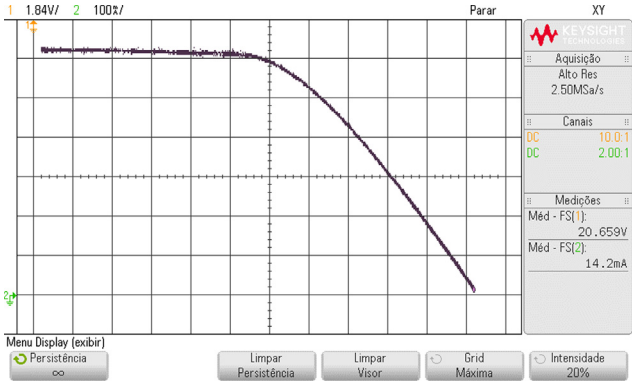

Fig. 13. *I–V* curve for $R_s = 5.82\ \Omega$ and $R_{sh} = 964\,\Omega$ ($S = 950\,W/m^2$ and $T = 40\,°C$) obtained experimentally.

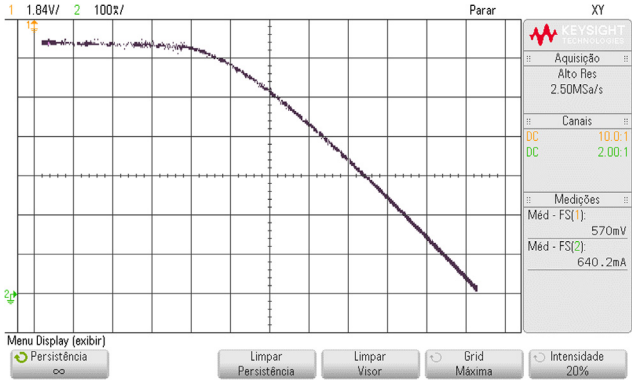

Fig. 14. *I–V* curve for $R_s = 15.82\ \Omega$ and $R_{sh} = 964\,\Omega$ ($S = 950\,W/m^2$ and $T = 40\,°C$) obtained experimentally.

maximum power is found to be about 9.6 W. Similarly, the external series resistance is increased to 5 Ω, 15 Ω, and 25 Ω in Fig. 13, Fig. 14, and Fig. 15, respectively.

Good compliance exists between simulation and experimental results, especially in terms of the shape expected for the *I-V* curve as the series resistance comes to vary. Besides, the maximum power that can be extracted from the PV module is reduced as R_s increases, which has direct impact on the voltage at the maximum power point. According to Tables 3 and 4, the ideality factor may even become negative at high values of R_s.

The maximum power voltage is progressively reduced from 17.22 V to 10.62 V, what could be a problem in real grid-connected systems, since the voltage across the dc-link of the dc-ac converter would be drastically reduced. This characteristic could make the use of the PV

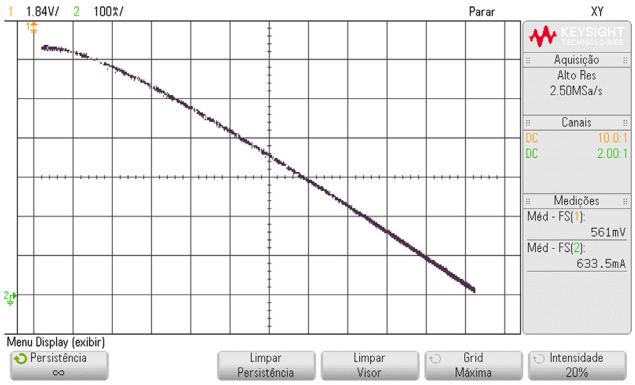

Fig. 15. *I–V* curve for $R_s = 25.82\ \Omega$ and $R_{sh} = 964\,\Omega$ ($S = 950\,W/m^2$ and $T = 40\,°C$) obtained experimentally.

Table 3
Parameters obtained from simulation (S = 950 W/m^2 and T = 40 °C).

R_s (Ω)	V_{OC} (V)	I_{SC} (A)	V_{MPP} (V)	I_{MPP} (A)	P_{MPP} (W)	A
0.82 Ω	20.7	0.6346	17.2250	0.5803	9.9956	1.3677
0.82 Ω + 1 Ω	20.7	0.6346	16.7180	0.5784	9.6704	1.1245
0.82 Ω + 5 Ω	20.7	0.6346	12.6220	0.5469	6.9025	0.1778
0.82 Ω + 15 Ω	20.7	0.6346	11.3750	0.4892	5.5648	−1.9994
0.82 Ω + 25 Ω	20.7	0.6346	10.6260	0.3572	3.7958	−3.8848

Table 4
Parameters obtained from experimental tests (S = 950 W/m^2 and T = 40 °C).

R_s (Ω)	V_{OC} (V)	I_{SC} (A)	V_{MPP} (V)	I_{MPP} (A)	P_{MPP} (W)	A
0.82 Ω	20.7	0.6346	17.2250	0.5803	9.9956	1.3677
0.82 Ω + 1 Ω	20.7	0.6346	16.7180	0.5784	9.6704	1.1245
0.82 Ω + 5 Ω	20.7	0.6346	12.6220	0.5469	6.9025	0.1778
0.82 Ω + 15 Ω	20.8	0.6350	11.2750	0.5000	5.6375	−1.8757
0.82 Ω + 25 Ω	20.8	0.6350	10.5260	0.3749	3.9462	−3.9172

module infeasible, since its respective output voltage would be lower than the rated value assumed at normal operating conditions when R_S is typically low. Depending on the inverter characteristics and the adopted MPPT technique, the reduction of 38% in the maximum power voltage would make the system operate far from the maximum power point.

Finally, it is worth to mention that the relative error in Table 5 is negligible when the series resistance is 0.82 Ω, 1.82 Ω, and 5.82 Ω since the *I-V* characteristics obtained experimentally and by simulation are overlapped, as the theoretical values shown in Table 3 have also been adopted in Table 4. However, as R_s increases to 15.82 Ω, and 25.82 Ω, both V_{MPP} and I_{MPP} tend to decrease and, consequently, the percent error increases, even though there are no significant differences when the absolute values of the aforementioned quantities are considered.

Table 5
Percent relative error for the parameters obtained from experimental tests and simulation (S = 950 W/m^2 and T = 40 °C).

R_s (Ω)	V_{OC} (%)	I_{SC} (%)	V_{MPP} (%)	I_{MPP} (%)	P_{MPP} (%)	A (%)
0.82 Ω	0	0	0	0	0	0
0.82 Ω + 1 Ω	0	0	0	0	0	0
0.82 Ω + 5 Ω	0	0	0	0	0	0
0.82 Ω + 15 Ω	0.481	0.063	0.887	2.160	1.29	1.102
0.82 Ω + 25 Ω	0.481	0.063	0.95	4.721	3.811	1.614

5. Conclusion

This work has presented a simple analytical expression for the calculation of the ideality factor in silicon PV modules. Even though many works in literature consider that such parameter remains constant, it has been effectively shown that it tends to decrease over time as influenced by the intrinsic series and shunt resistances.

According to the developed analysis, it can be stated that the ideality factor is mainly influenced by the increase of the series resistance, which is often associated to corrosion and performance degradation as a consequence of the aging process of the PV module. As a consequence, the maximum power that can be extracted from the device is reduced, with direct impact on the performance of the whole PV conversion system. For instance, if the aging of commercial module KM(P)10 is emulated with the significant increase of R_s from 0.82 Ω to 25.82 Ω, the maximum power will be reduced by 60.5%. This is due to the drastic reduction of the voltage and current ratings at the maximum power point as demonstrated in both simulation and experimental tests, as good agreement between them is achieved.

Acknowledgement

The authors would like to acknowledge INERGE and also Brazilian research funding agencies CAPES, CNPq, and FAPEMIG for the support to this work.

References

[1] Jones DC, Erickson RW. Probabilistic analysis of a generalized perturb and observe algorithm featuring robust operation in the presence of power curve traps. IEEE Trans Power Electron 2013;28:2912–26.
[2] Rahman SA, Varma RK, Vanderheide T. Generalised model of a photovoltaic panel. IET Renew Power Gener 2014;8:217–29.
[3] Chin VJ, Salam Z, Ishaque K. An accurate modelling of the two-diode model of PV module using a hybrid solution based on differential evolution. Energy Convers Manage 2016;124:42–50.
[4] Adamo F, Attivissimo F, Nisio AD, Spadavecchia M. Characterization and testing of a tool for photovoltaic panel modeling. IEEE Trans Instrum Meas 2011;60:1613–22.
[5] Gomes RCM, Vitorino MA, Corrêa MBdR, Fernandes DA, Wang R. Shuffled complex evolution on photovoltaic parameter extraction: a comparative analysis. IEEE Trans Sustainable Energy 2017;8:805–15.
[6] Hejri M, Mokhtari H, Azizian MR, Ghandhari M, Söder L. On the parameter extraction of a five-parameter double-diode model of photovoltaic cells and modules. IEEE J Photovoltaics 2014;4:915–23.
[7] Soon JJ, Low KS. Optimizing photovoltaic model for different cell technologies using a generalized multidimension diode model. IEEE Trans Ind Electron 2015;62:6371–80.
[8] Batzelis EI, Kampitsis GE, Papathanassiou SA, Manias SN. Direct MPP calculation in terms of the single-diode PV model parameters. IEEE Trans Energy Convers 2015;30:226–36.
[9] Batzelis EI, Papathanassiou SA. A method for the analytical extraction of the single-diode PV model parameters. IEEE Trans Sustainable Energy 2016;7:504–12.
[10] Shongwe S, Hanif M. Comparative analysis of different single-diode PV modeling methods. IEEE J Photovoltaics 2015;5:938–46.
[11] Villalva MG, Gazoli JR, Filho ER. Comprehensive approach to modeling and simulation of photovoltaic arrays. IEEE Trans Power Electron 2009;24:1198–208.
[12] Picault D, Raison B, Bacha S, de la Casa J, Aguilera J. Forecasting photovoltaic array power production subject to mismatch losses. Sol Energy 2010;84:1301–9.
[13] Cuce E, Cuce PM, Karakas IH, Bali T. An accurate model for photovoltaic (PV) modules to determine electrical characteristics and thermodynamic performance parameters. Energy Convers Manage 2017;146:205–16.
[14] Ghani F, Duke M, Carson J. Numerical calculation of series and shunt resistances and diode quality factor of a photovoltaic cell using the Lambert W-function. Sol Energy 2013;91:422–31.
[15] Daliento S, Lancellotti L. 3D Analysis of the performances degradation caused by series resistance in concentrator solar cells. Sol Energy 2010;84:44–50.
[16] Rahman MM, Hasanuzzaman M, Rahim NA. Effects of various parameters on PV-module power and efficiency. Energy Convers Manage 2015;103:348–58.
[17] Bayhan H, Bayhan M. A simple approach to determine the solar cell diode ideality factor under illumination. Sol Energy 2011;85:769–75.
[18] Subudhi B, Pradhan R. A comparative study on maximum power point tracking techniques for photovoltaic power systems. IEEE Trans Sustainable Energy 2013;4:89–98.
[19] Kim KA, Xu C, Jin L, Krein PT. A dynamic photovoltaic model incorporating capacitive and reverse-bias characteristics. IEEE J Photovoltaics 2013;3:1334–41.
[20] Bashahu M, Nkundabakura P. Review and tests of methods for the determination of the solar cell junction ideality factors. Sol Energy 2007;81:856–63.
[21] Ozkartal A, Temirci C. Relationship between photovoltaic and diode characteristic parameters in the Sn/p-Si Schottky type photovoltaics. Sol Energy 2016;132:96–102.
[22] Tabish S, Ashraf I. Performance evaluation of PV module under various parametric conditions. Int J Ambient Energy 2017:1–6.
[23] Park HK, Choi J. Origin of voltage-dependent high ideality factors in graphene–-silicon diodes. Adv Electron Mater 2018;4:1700317.
[24] Öğütman K, Davis KO, Schneller E, Yelundur V, Schoenfeld WV. Integration of spatially resolved ideality factor into local cell efficiency analysis with photoluminescence. Sol Energy 2017;158:869–74.
[25] Fortes M, Comesaña E, Rodriguez JA, Otero P, Garcia-Loureiro AJ. Impact of series and shunt resistances in amorphous silicon thin film solar cells. Sol Energy 2014;100:114–23.
[26] Ruschel CS, Gasparin FP, Costa ER, Krenzinger A. Assessment of PV modules shunt resistance dependence on solar irradiance. Sol Energy 2016;133:35–43.
[27] Coelho RF, Concer F, Martins DC. A proposed photovoltaic module and array mathematical modeling destined to simulation. In: 2009 IEEE international symposium on industrial electronics; 2009. p. 1624–9.
[28] Sera D, Teodorescu R, Rodriguez P. Photovoltaic module diagnostics by series resistance monitoring and temperature and rated power estimation. In: 2008 34th annual conference of IEEE industrial electronics; 2008. p. 2195–9.
[29] Wirth H, Weiß K-A, Wiesmeier C. Photovoltaic modules – technology and reliability, 1st ed., deGruyter; 2016.
[30] Wolf P, Benda V. Identification of PV solar cells and modules parameters by combining statistical and analytical methods. Sol Energy 2013;93:151–7.
[31] Gasparin FP, Bühler AJ, Rampinelli GA, Krenzinger A. Statistical analysis of I-V curve parameters from photovoltaic modules. Sol Energy 2016;131:30–8.
[32] KOMAES. (Octobert, 1st). Solar module – KM(P)10. Available: < http://www.solarbrasil.com.br/images/solarbrasil/downloads/KM_10.pdf > .
[33] Sera D, Teodorescu R. Robust series resistance estimation for diagnostics of photovoltaic modules. In: 2009 35th annual conference of IEEE industrial electronics; 2009. p. 800–5.
[34] Arab AH, Bakelli Y, Semaoui S, Bandou F, Mahammed IH. Long term performance of crystalline silicon photovoltaic modules. In: 2015 3rd international renewable and sustainable energy conference (IRSEC); 2015. p. 1–5.
[35] Ghanbari T. Hot spot detection and prevention using a simple method in photovoltaic panels. IET Gener Transm Distrib 2017;11:883–90.